Original Article

Novel dominant-negative *FOXJ1* mutation in a family with heterotaxy plus mouse model

Lulu Li[1#^], Guocheng Shi[2#], Xingyu Zhang[1#], Teng Wang[3], Bo Wang[1,4], Yunqian Gao[1,4], Guoling You[4,5], Qihua Fu[1,4], Ying Xiang[1,4], Xiaoqing Zhang[1,4^]

[1]Pediatric Translational Medicine Institute, Shanghai Children's Medical Center, Shanghai Jiao Tong University School of Medicine, Shanghai, China; [2]Department of Cardiothoracic Surgery, Congenital Heart Center, Shanghai Children's Medical Center, Shanghai Jiao Tong University School of Medicine, Shanghai, China; [3]Shanghai Institute of Precision Medicine, Shanghai Ninth People's Hospital, Shanghai Jiao Tong University School of Medicine, Shanghai, China; [4]Shanghai Key Laboratory of Clinical Molecular Diagnostics for Pediatrics, Shanghai, China; [5]Department of Laboratory Medicine, Shanghai Children's Medical Center, Shanghai Jiao Tong University School of Medicine, Shanghai, China

Contributions: (I) Conception and design: Xiaoqing Zhang, Y Xiang, Q Fu; (II) Administrative support: None; (III) Provision of study materials or patients: G Shi; (IV) Collection and assembly of data: Xingyu Zhang, T Wang, B Wang, Y Gao, G You; (V) Data analysis and interpretation: L Li, Xiaoqing Zhang; (VI) Manuscript writing: All authors; (VII) Final approval of manuscript: All authors.

[#]These authors contributed equally to this work.

Correspondence to: Xiaoqing Zhang, PhD; Ying Xiang, PhD; Qihua Fu, PhD. Pediatric Translational Medicine Institute, Shanghai Children's Medical Center, Shanghai Jiao Tong University School of Medicine, Shanghai 200127, China; Shanghai Key Laboratory of Clinical Molecular Diagnostics for Pediatrics, Shanghai, China. Email: qingxiao18@163.com; 1262975038@qq.com; qfu@shsmu.edu.cn.

Background: Primary ciliary dyskinesia (PCD) is a clinically heterogeneous group of autosomal or, less frequently, X-chromosomal recessive inheritance syndrome of motile cilia dysfunction characterized by neonatal respiratory distress, oto-sino-pulmonary disease, infertility and situs inversus. Recently, type 43 PCD (CILD43, OMIM#618699) was established by autosomal-dominant loss-of-function mutations identified in Forkhead box J1 (*FOXJ1*). However, the functional validation of *FOXJ1* mutations in humans and mice has not been fully performed. Here we studied a three-generation family with heterotaxy and proband with complex congenital heart disease (CHD).

Methods: We performed whole-exome sequencing to investigate the causative variant of this family and generated gene knock-in mice carrying the human equivalent mutation by homologous recombination. Then, microscopy analysis was used to characterize the phenotype and ciliary ultrastructure of the model. Effects of the variant on heart anomaly were preliminarily explored through transcriptome sequencing.

Results: A novel heterozygous deletion variant (c.1129delC/p.Leu377Trpfs*76) of *FOXJ1* was discovered that exerts a dominant-negative effect (DNE) *in vitro*. Notably, both homozygous (*Foxj1*$^{c.1129delT/c.1129delT}$) and heterozygous (*Foxj1*$^{+/c.1129delT}$) mice developed situs inversus, hydrocephalus and showed a disruption of trachea cilia structure, whereas these abnormalities were only observed in previously reported *Foxj1*$^{-/-}$, not *Foxj1*$^{+/-}$ mice. Thus, a more severe phenotype and higher expressivity of our mouse model further indicated the DNE of this mutation. Meanwhile, several cardiomyopathy-related genes were differentially expressed in the homozygous *Foxj1* knock-in mouse hearts, pointing to a probable function in cardiac pathology.

Conclusions: Overall, our study results showed that c.1129delC mutation in *FOXJ1* was regarded as the cause of situs inversus in this family and this mutant showed a capacity of DNE over wild-type FOXJ1, causing more serious consequences than the allelic deletion of *Foxj1*.

Keywords: *FOXJ1*; deletion mutation; dominant-negative effect; type 43 primary ciliary dyskinesia; congenital heart disease

^ ORCID: Lulu Li, 0000-0002-5129-784X; Xiaoqing Zhang, 0000-0002-2106-2994.

Submitted Jan 13, 2023. Accepted for publication Jul 28, 2023. Published online Aug 28, 2023.
doi: 10.21037/tp-23-27
View this article at: https://dx.doi.org/10.21037/tp-23-27

Introduction

Primary ciliary dyskinesia (PCD, OMIM#244400) is a rare inherited motile ciliopathy, characterized by upper and lower respiratory tract disease, organ laterality defects, subfertility, and hydrocephalus due to the defective ciliary apparatus (1). Over 40 genes have been reported to cause PCD, an autosomal recessive or, less frequently, X-chromosomal recessive inheritance pattern disorder (2). In 2019, type 43 PCD (CILD43, OMIM#618699) was created by *de novo* autosomal-dominant loss-of-function mutations identified in Forkhead box J1 (*FOXJ1*) from six sporadic cases (3). Subsequently, six unrelated individuals harboring heterozygous variants in *FOXJ1* were described in two separate studies (4,5). The phenotypic presentation of these patients encompasses the expected symptoms of a multisystem motile ciliary defect, but exhibits a remarkably variability and expressivity, involving the central nervous system, the respiratory system and other systems (6). So far, only eight *FOXJ1* variants have been reported in individuals with PCD or hydrocephalus, and the functional roles of these mutants have rarely been studied. Moreover, additional patients carrying mutations in *FOXJ1* with unusual phenotypic presentation could promote a deeper understanding of the functional basis of this gene.

FOXJ1, also known as HFH-4, a member of the forkhead family of transcription factors, is mainly expressed in motile ciliated cells, where as a master regulator of the ciliogenic program (7). Numerous researches have revealed a pivotal role of *FOXJ1* in many tissues that possess highly ciliated cells, such as conducting airways, choroid plexus, ependyma of the brain, testis, and oviduct (8-10) as well as motile mono-cilia in the embryonic left/right organizer (LRO) (11,12). Consistently, gene modifications in animal models and mutations identified in humans have demonstrated that *FOXJ1* dysfunction impairs ciliary action in specific zones causing a variety of genetic disorders (3,13) including hydrocephalus (14), laterality phenotypes (11) and mucociliary clearance disorder (15) due to a dramatic number reduction of motile cilia and axoneme structure severe defects (11,13). Yet, *Foxj1* knock-in mouse model corresponding to human mutation identified in CILD43 cases has not been reported and limited information is currently known about the underlying molecular mechanisms.

In this study, we characterized a family with heterotaxy and the proband with complex congenital heart disease (CHD). A heterozygous variant c.1129delC (p.Leu377Trpfs*76) in *FOXJ1* was identified. We found that this mutant exhibited a dominant-negative effect on the transcriptional activity of *RFX3*, downstream of *FOXJ1* in the node, and cooperatively induce the expression of ciliated genes (16). The transcription factor RFX3 directs nodal cilium development and left-right asymmetry specification (17). Mice carrying the equivalent of the human *FOXJ1*-c.1129delC mutation were generated and found to have disrupted motile cilia structure in trachea epithelial cells and randomized left-right patterning and hydrocephalus. Meanwhile, transcriptome results of this knock-in mouse heart tissues point to some genes involved in cardiac pathology, which may provide clues for the role of *FOXJ1* in heart disease. We present this article in accordance with the ARRIVE reporting checklist (available at https://tp.amegroups.com/article/view/10.21037/tp-23-27/rc).

Highlight box

Key findings

- Identification of a novel heterozygous deletion variant, c.1129delC, in *FOXJ1* (p.Leu377Trpfs*76) in a Chinese family with type 43 primary ciliary dyskinesia (CILD43).

What is known and what is new?

- FOXJ1 is a master regulator of the ciliogenic program, and loss-of-function mutations in *FOXJ1* have been related to human primary ciliary dyskinesia.
- In this study, the first *Foxj1* knock-in mice were generated and recapitulated the ciliopathies of our patients. Our research revealed that c.1129delC variant exerts a dominant-negative effect and provided some ideas for the role of *FOXJ1* in heart disease.

What is the implication, and what should change now?

- Previous report supposed that haploinsufficiency of *FOXJ1* may be the cause of CILD43. Thus, more research is needed to understand the action mechanism of *FOXJ1* variants. In addition, CILD43 patients should be aware of the cardiac abnormality and CHD individuals could test for *FOXJ1* variants.

Methods

Family and patient

A non-consanguineous Chinese Han family from Anhui Province was recruited for our study. The proband was a 51-day-old boy with dextrocardia who was found to have complex congenital heart disease. His diagnoses were confirmed by echocardiography, cardiac catheterization examinations, computed tomography, and other operation recordings. His affected mother has total situs inversus visceral. Clinical features were checked at Shanghai Children's Medical Center (SCMC). The study was conducted in accordance with the Declaration of Helsinki (as revised in 2013). The study was approved by the Ethics Committee of the Shanghai Children's Medical Center (SCMC) (No. SCMC-201015) and written informed consent was obtained from the parents of the child.

Whole-exome sequencing for candidate gene identification

Peripheral blood samples of all cases were collected, and genomic DNA was extracted using QIAamp® DNA Blood Mini Kit (QIAGEN, Hilden, Germany) by standard protocols. Exome sequencing was performed on the proband (III:1) and his parents (II:2, II:3) using the Agilent SureSelect capture kits (Agilent, Santa Clara, CA, USA). The captured libraries were subsequently sequenced using the Illumina HiSeq 2500 system. Sequencing data alignment and variant calling were performed as previously described (18). Given the nature of primary ciliary dyskinesia (PCD) genetics, we began to search for variants in known PCD-causing genes, considering rare truncating and missense variants. The pathogenicity of variants was evaluated using American College of Medical Genetics and Genomics (ACMG) standards and guidelines (19). *FOXJ1*-c.1129delC (p.L377Wfs*76) was classified as pathogenic based on the evidence of 1 very strong (PVS1) and 1 strong (PS2) and 1 moderate (PM2). Co-segregation with the phenotype were confirmed by Sanger sequencing. PCR primers are listed in Table S1.

Plasmid construction

The coding region of the wild-type (WT) and mutant (p.Leu377Trpfs*76) *FOXJ1* containing a partial 3' untranslated region were cloned into pcDNA3.1 vector with a flag-tagged sequence in the 3' end. The human *RFX3* promoter sequence (chr9:3,525,790-3,527,302, hg38) was cloned into the pGL4.10 vector (Promega, Madison, USA) to produce RFX3-promoter-Luc. All constructs were validated by Sanger sequencing.

Cell culture and transfection

HEK 293T cell line was obtained from the cell bank of the Committee on Type Culture Collection of the Chinese Academy of Sciences (Shanghai, China) and cultured in high-glucose Dulbecco Modified Eagle Medium (#11965092, Gibco™) supplemented with 10% fetal bovine serum (#10099141, Gibco™) at 37 ℃ with 5% CO_2. Transient transfection was performed with Lipofectamine 3000 Transfection Reagent (#L3000008, Invitrogen™) according to the manufacturer's protocol.

Western blot and immunofluorescence

HEK293T cells were seeded in 12-well plates, transiently transfected with WT or mutant FLGA-FOXJ1 vectors, and lysed after 48 hours using sodium dodecyl sulfate (SDS) buffer for Western blot analyses. Polyvinylidene difluoride (PVDF) membranes were incubated with primary anti-FLAG antibody (#14793, CST) and loading control antibody GAPDH (#5174, CST), followed by anti-rabbit IgG secondary antibodies conjugated to horseradish peroxidase, then detected with the chemiluminescence system. Protein band intensities were quantified by ImageJ software (version 1.53t, National Institutes of Health, USA). For immunofluorescence staining, transfected HEK293T cells were fixed using 4% paraformaldehyde/phosphate-buffered saline (PFA/PBS) for 20 min, rinsed with PBS, permeabilized with 1% TritonX-100/PBS for 10 min, and blocked with 1% bovine serum albumin/PBS solution for 30 min at room temperature. The treated cells were incubated with anti-FLAG antibody at a dilution of 1:1,000 and then washed three times with PBS, followed by incubation with fluorescein isothiocyanate conjugated secondary antibody for 1 h. Finally, nuclei were stained with 4,6-diamidino-2-phenylindole (DAPI), and images were captured using a Laser Scanning Confocal Microscope.

Dual-luciferase reporter assay

RFX3-Luc Photinus pyralis luciferase reporter plasmid, WT/mutant *FOXJ1* constructs or empty vector, and internal control Renilla luciferase reporter plasmid pRL-TK were co-transfected in HEK293T cells. Briefly, HEK293T

cells were transiently transfected for 24 hours using Lipofectamine 3000 with 200 ng of the RFX3-Luc, 20 ng of Renilla pRL-TK, and co-transfected with either: 150 ng pcDNA3.1 (empty vector); 75 ng pcDNA3.1 and 75 ng of WT *FOXJ1*; 75 ng pcDNA3.1 and 75 ng mutant *FOXJ1*; and 75 ng WT *FOXJ1* plus 75 ng mutant *FOXJ1*. Both luciferase activities were determined using the Dual-Glo® Luciferase Assay System (#E2920, Promega) according to the supplier's recommendations, and then data were expressed as the ratio of firefly/Renilla luciferase activity. Experiments were performed three times independently with three technical triplicates each.

Generation and histological analysis of Foxj1-c.1129delT mice

Briefly, the *Foxj1*-c.1129delT targeting construct was linearized by restriction digestion with NotI followed by phenol/chloroform extraction and ethanol precipitation. The linearized vector was transfected into C57BL/6N embryonic stem cells (ESC) according to Cyagen's (Suzhou, China) standard electroporation procedures. Positive ESC clone was injected into C57BL/6 albino embryos, then re-implanted into CD-1 pseudo-pregnant females. Founder animals were identified by their coat color, and their germline transmission was confirmed by breeding with C57BL/6 females and subsequent genotyping of the offspring. The Neo cassette, flanked by SDA (self-deletion anchor) sites, is self-deleted in germ cells, thus, so the offspring is Neo cassette-free. Genotyping was confirmed on mouse tail snip DNA by Sanger sequencing. All experiments were performed under a project license (No. SCMC-LAWEC-2023-005) granted by institutional Animal Care and Use Committee of SCMC, in compliance with SCMC institutional guidelines for the care and use of animals. The sample size, genotype and age of the experimental models are indicated in the legends. At same age mice of each genotype were divided into groups for comparative analysis. No other treatment was given to the mice and no inclusion and exclusion were set. Mouse brains were collected and fixed in 4% PFA/PBS overnight, then were processed for paraffin embedding, sectioned at a thickness of 5 μm, and stained with hematoxylin-eosin using our reported procedures (18). Stained sections were imaged with a Leica DM6000 microscope.

Electron microscopy (EM)

Mouse trachea was isolated and prefixed with 2.5% (vol/vol) glutaraldehyde in 0.2 M phosphate buffer overnight at 4 ℃, washed and then post-fixed in 1% (wt/vol) osmium tetroxide for 1.5 h. Samples were prepared following standard transmission electron microscope (TEM) and scanning electron microscopy (SEM) protocols. We randomly watched three hundred cilia for each sample using twenty different microscope fields, but only those that could clearly distinguished between the normal and abnormal ciliary ultrastructure were counted and used for statistical analysis from about one hundred cilia. Ultrastructural abnormalities of the microtubule arrangement were counted by an expert.

RNA-Seq analysis

Total RNA isolated from the postnatal day 1 (P1) heart of three WT and three *Foxj1*$^{c.1129delT/c.1129delT}$ mice was for RNA sequencing, respectively. Library preparation and RNA-seq were performed on the NovaSeq 6000 System to generate 150 bp paired-end reads by Berry Genomics Corporation Ltd (Beijing, China). Clean reads were aligned to the reference genome (mm10) by HISAT2. DESeq2 package was used for differential expression genes (DEGs) analysis as we did before (20). Gene Ontology (GO) and KEGG pathway analysis of the DEGs were performed using the The Database for Annotation, Visualization and Integrated Discovery (DAVID) Bioinformatics Resources and its functional annotation tools (https://david.ncifcrf.gov/home.jsp).

Statistical analysis

GraphPad Prism (version 9.4.1, USA) was used for statistical analysis. The data for the comparison of two groups were analyzed using the independent samples *t*-test, and one-way analysis of variance (ANOVA) was used to compare data for three or more groups. $P<0.05$ was considered statistically significant.

Results

Clinical features and mutation analysis

In this study, a Chinese family with heterotaxy was identified (*Figure 1A*,*1B*). The proband (III:1) was a 51-day-old boy who had dextrocardia and was born with complex congenital heart disease including total anomalous pulmonary venous connection (TAPVC), atrial septal defect, pulmonary valve stenosis, and atrioventricular septal defect. He underwent a primary TAPVC repair with concomitant PA banding

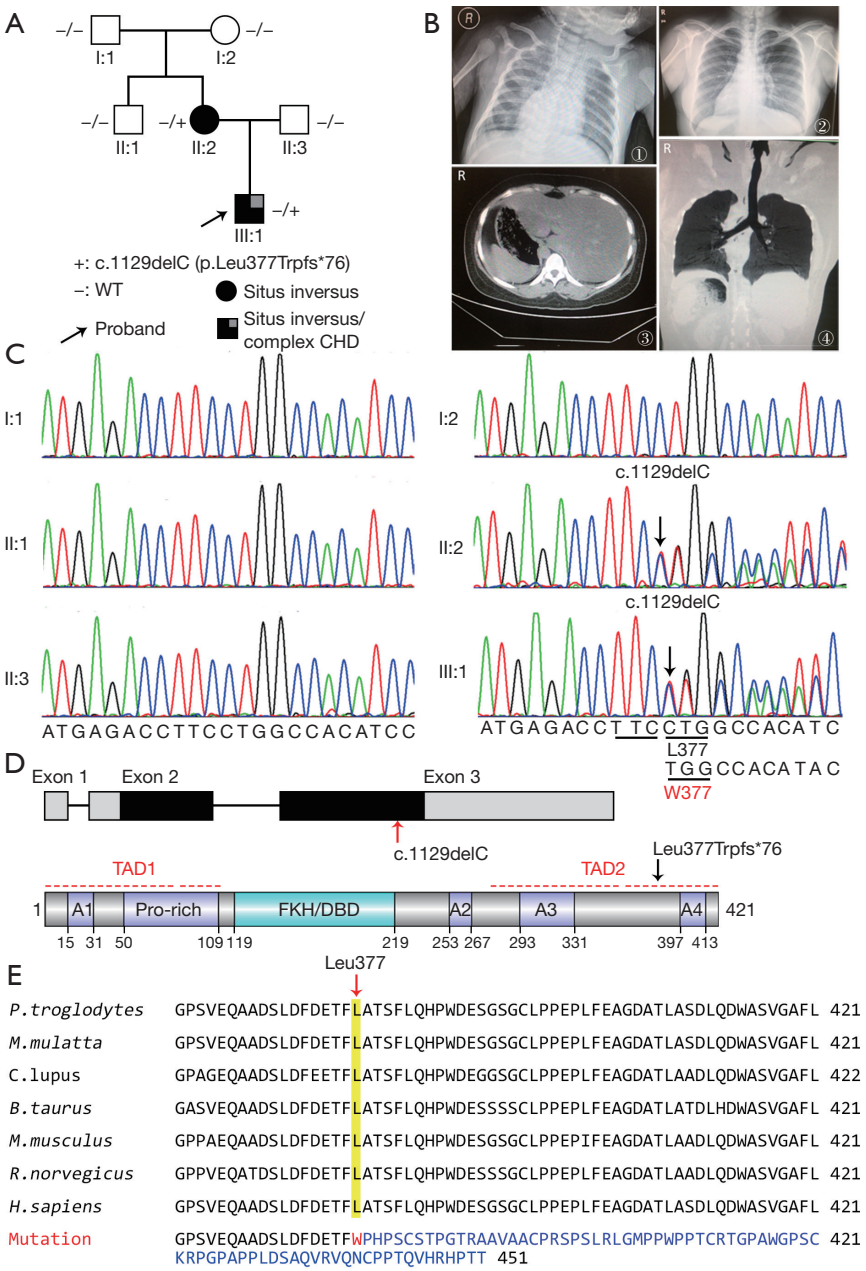

Figure 1 Identification of a novel heterozygous variant in *FOXJ1* in the reported family. (A) The pedigree of the family with situs inversus/ CHD. Squares and circles indicate males and females, respectively. Filled symbols indicate affected individuals, and open symbols indicate unaffected individuals. (B) Radiological examination of the proband (III:1) and his mother (II:2). Preoperative chest X-ray showed dextrocardia in III:1 (B1). Chest X-ray showed dextrocardia in II:2 (B2). Cross-sectional CT image revealed that II:2 had situs inversus totalis with the stomach on the right and the liver on the left (B3). CT coronal scan showed that II:2 had situs inversus totalis, including bronchial situs, left-sided liver, and right-sided stomach (B4). (C) Electropherograms of Sanger sequencing results of *FOXJ1*-c.1129delC variant for the family members. (D) Schematic structure of the FOXJ1 gene and the FOXJ1 protein. *FOXJ1* consists of two coding exons and encoding a 421aa protein. c.1129delC variant located in Exon3 and indicated with a red arrow. FOXJ1 includes four acidic amino acid residues rich regions (A1-A4), a proline-rich region (Pro-rich), a forkhead DNA binding domain (FKH/DBD), and two transactivation domains (TAD1 and TAD2) (10). (E) Conservation analyses of residue 377 in FOXJ1 among different species by multiple sequence alignments and the predicted amino acid sequence consequence of c.1129delC variant for *FOXJ1*. *FOXJ1*, Forkhead box J1; CHD, congenital heart disease; CT, computed tomography.

at 2-month-old, and subsequently a bidirectional Glenn procedure was performed at age of 1 year and postoperative monitoring showed an enhanced and blurred, and exudation in both lungs. This patient had progressive pulmonary hypertension and died of heart failure at 2.5 years of age. His mother (II:2) exhibited total situs inversus, and she was infertile that get pregnant by assisted reproductive technologies. These disease phenotypes are not seen in other family members. The proband reported a history of thick breathing sounds in both lungs after birth. To identify the causal genetic responsible for the disorders in this family, whole exome sequencing of the proband (III:1) and his parents (II:2 and II:3) were conducted. Based on the sequencing data, a heterozygous variant c.1129delC in *FOXJ1* (RefSeq accession number NM_001454.4) was found in the proband and his affected mother. Further, we performed Sanger sequencing for two affected members (II:2 and III:1) and four unaffected members (I:1, I:2, II:1 and II:3) and confirmed c.1129delC variant co-segregation with the misplaced organ phenotype (*Figure 1C*). This deletion variant is predicted to lead to a shift in the reading frame at codon 377 (Leu377Trp) and altered the last 45 amino acids (aa), abolished the original stop codon (422Ter), and added 30aa (p.Leu377Trpfs*76) to the carboxyl-terminal transactivation domain (TAD) of FOXJ1 (*Figure 1D*). The protein sequence alignment showed that Leu377 through the remaining amino acids (377-421aa) of human FOXJ1 is highly conserved among mammals (*Figure 1E*). Moreover, the *FOXJ1*-c.1129delC variant has not previously been reported in ClinVar, ExAC, genomAD, and 1,000 Genomes databases and was classified as a pathogenic variant according to the ACMG guidelines.

*The p.Leu377Trpfs*76 mutation did not affect FOXJ1 expression levels and subcellular localization*

To evaluate the functional consequence of the *FOXJ1*-c.1129delC mutation, we first detected the protein expression level and cellular localization of FLAG-FOXJ1-WT and -Leu377Trpfs*76 (p.L377Wfs*76) in HEK293T cells. Consistent with the predicted result that 30 more amino acids of FOXJ1 (mutant: 451aa) were produced than wild-type (WT) due to the c.1129delC mutation. We observed a higher molecular weight band of mutants and showed no significant difference in protein expression levels when compared to WT FOXJ1 according to the western blot analysis (*Figure 2A*,*2B*). Moreover, we found that both WT and mutant FOXJ1 proteins were explicitly localized in the nucleus (*Figure 2C*). These results show that *FOXJ1*-c.1129delC mutation produced longer non-canonical stable proteins with normal subcellular distribution as WT proteins are.

The FOXJ1 mutant has a dominant-negative effect on the RFX3 transcriptional activity

RFX3 is a key downstream of FOXJ1, interacts and functions as a co-activator with FOXJ1 to regulate the expression of cilia-related genes. Thus, we focused on studying the effect of FOXJ1-Leu377Trpfs*76 mutant on the transcriptional activity of *RFX3*. HEK293T cells transfected with plasmids encoding WT FOXJ1, empty vector, and reporter plasmid showed an approximately 4.1-fold higher luciferase activity than cells transfected with empty vector alone (Vector: 0.49±0.01; WT: 1.91±0.11). Transfection of HEK293T cells with FOXJ1 mutant led to a luciferase activity that was about 1.5-fold higher than the empty vector and was significantly reduced to 39%±11% compared with WT under the same experimental conditions (p.Leu377Trpfs*76: 0.74±0.04). However, when the plasmids encoding WT and mutant FOXJ1 were co-transfected (WT/p.Leu377Trpfs*76: 1.31±0.09), the reporter activity was reduced to 69%±9% of WT alone. Additionally, a significant luciferase activity after transfection of a mock vector could be due to endogenous FOXJ1 expression in HEK293T cells (*Figure 2D*). Thus, our dual-luciferase reporter assay results indicate that the FOXJ1 mutant exerts a dominant-negative effect on the *RFX3* transcriptional activity.

Generation and phenotypic characterization of Foxj1-c.1129delT knock-in mice

To model the human phenotype *in vivo* and further elucidate the potential underlying mechanisms, we generated a knock-in mouse carrying a mutation c.1129delT in *Foxj1* (orthologous mutation c.1129delC in human) by homologous recombination using a targeting vector containing exons 2 to 3 (*Figure 3A*). This alteration was also predicted to lead to a longer non-functional protein production (p.Leu377Trpfs*84, Figure S1). Heterozygous pups ($Foxj1^{+/c.1129delT}$) were born at the expected Mendelian frequency, yet exhibited dramatic growth retardation, and all died within 2 months after birth with a mean survival time of 28 days (*Figure 3B*). In addition, $Foxj1^{+/c.1129delT}$ mice developed hydrocephalus at about 2 weeks of age

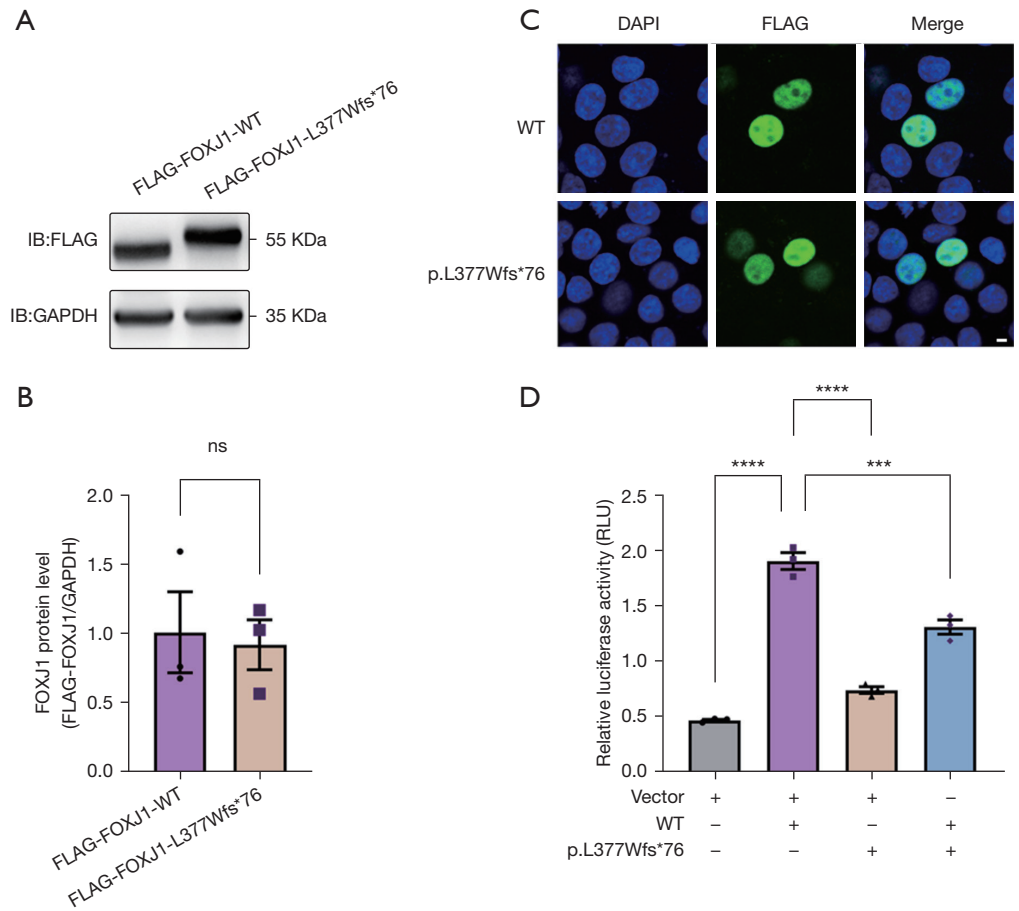

Figure 2 Functional analysis of the wild-type and mutant FOXJ1 protein. (A) The protein expression level of FOXJ1-WT and -L377Wfs*76. GAPDH is used as an internal control. (B) Quantification of FLAG-FOXJ1/GAPDH. Significance was determined with the two-tailed unpaired *t*-test, ns, no significance, P>0.05. (C) Immunofluorescence staining photography shows the localization of WT and mutant FOXJ1 in HEK293T cells. Scale bar, 7.5 μm. (D) p.L377Wfs*76 mutant influence the transcriptional activity of *RFX3*. Significance was determined with the one-way ANOVA, ***, P<0.001, ****, P<0.0001. All the data are presented as mean ± standard error of mean from three replicate experiments. FOXJ1, Forkhead box J1; WT, wild-type; RLU, relative light units; ANOVA, analysis of variance.

and displayed abnormal head morphology with complete penetrance by 2 months (*Figure 3C*,*3D*). Homozygous (*Foxj1*$^{c.1129delT/c.1129delT}$) mutation results in neonatal lethality in mice accompanied by severe hydrocephalus and few could survive 1 week (*Figure 3E*). Moreover, WT mice show completely normal organ placement and cardiac apical position. However, the *Foxj1*-c.1129delT mutants with dextrocardia or mirror image reversal of internal organ situs (*Figure 3F*). 11% (2 of 18 mutants) of the heterozygous mice showed laterality defects, such as situs inversus totalis or heterotaxis, and homozygous mutants presented with situs inversus at a rate of 71% (5 of 7 mutants) in live births based on the position of the heart and stomach (*Figure 3G*). Our results demonstrated that compared with WT mice, *Foxj1*-c.1129delT knock-in mice died early and presented with hydrocephalus and randomization of left/right body asymmetry.

Foxj1-c.1129delT mice show reduced numbers of cilia and defective ciliary ultrastructure

Cilia have been implicated in the development of hydrocephalus and the determination of asymmetry of the heart and visceral organs. Hence, we characterized the ciliary morphology and ultrastructure in *Foxj1*-c.1129delT mutant mouse trachea epithelial cells. Immunofluorescence (IF) microscopy analyses with antibodies targeting acetylated-tubulin (a marker of the ciliary axonemes) and

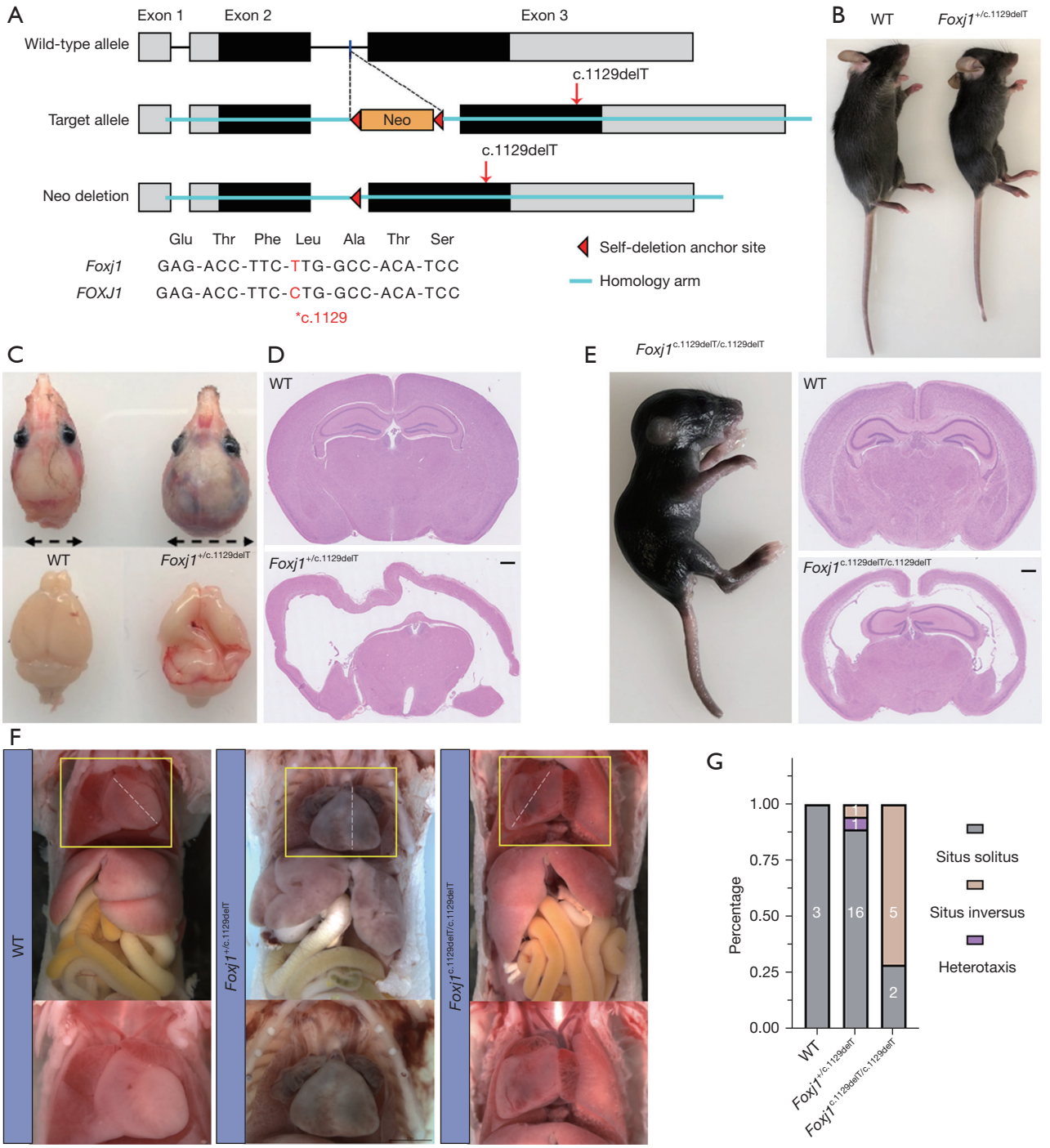

Figure 3 Generation and phenotype description of *Foxj1*-c.1129delT knock-in mice. (A) Schematic representation of the targeting strategy for producing *Foxj1*-c.1129delT knock-in mice. (B) The general appearance of WT and *Foxj1*$^{+/c.1129delT}$ mice. (C,D) Gross morphology (C) and HE stained sections (D) of postnatal days 28 WT and *Foxj1* mouse brains. Scale bar, 500 μm. (E) General appearance and HE stained sections of WT and *Foxj1*$^{c.1129delT/c.1129delT}$ mouse brains. (F) Dissections of 3-week-old WT, *Foxj1*$^{+/c.1129delT}$ and *Foxj1*$^{c.1129delT/c.1129delT}$ mice. The enlarged view and dashed line showed the direction of the heart apex of WT, *Foxj1*$^{+/c.1129delT}$ and *Foxj1*$^{c.1129delT/c.1129delT}$ mice, respectively. (G) The frequencies of aberrant organ placement in mice of the indicated genotypes. The number of mice present in each bar. FOXJ1, Forkhead box J1; WT, wild-type; HE, hematoxylin and eosin.

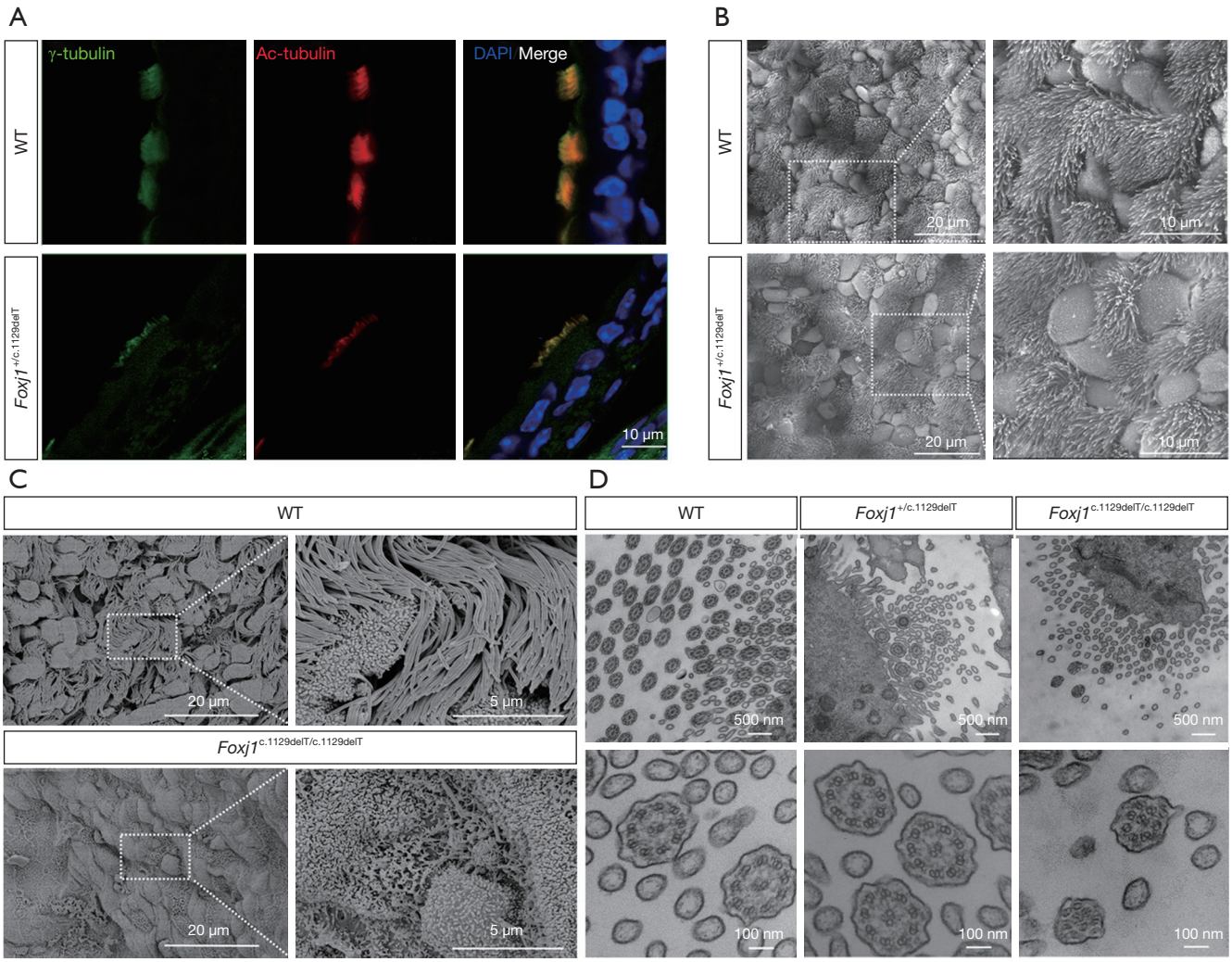

Figure 4 Tracheal cilia of *Foxj1*-c.1129delT mutant mice. (A, B) Trachea sections from WT and *Foxj1*$^{+/c.1129delT}$ mice were examined by immunofluorescence staining (A) and SEM (B). γ-tubulin, green; Ac-tubulin, red; nuclei are stained with DAPI (blue). (C) SEM images of the ciliated cells from WT and *Foxj1*$^{c.1129delT/c.1129delT}$ mouse tracheal sections (P7). (D) TEM image of a cross-section of the tracheal cilia from WT, *Foxj1*$^{+/c.1129delT}$, and *Foxj1*$^{c.1129delT/c.1129delT}$ mice. WT, wild-type; SEM, scanning electron microscopy; Ac-, acetylated; DAPI, 4,6-diamidino-2-phenylindole; TEM, transmission electron microscope.

γ-tubulin (a marker of the centrosome) showed reduced numbers and densities of trachea cilia and disorganized along the surface of trachea epithelial cells in *Foxj1*$^{+/c.1129delT}$ mice as the images displayed with scanning electron microscopy (SEM), while the WT mouse cilia signal was continuously observed and well-organized along the surface of trachea epithelial cells (*Figure 4A*,*4B*). The homozygous *Foxj1*$^{c.1129delT/c.1129delT}$ mutant mouse exhibited a significant reduction in tracheal cilia and far fewer and shorter cilia formed in contrast to the abundant, long broom-like cilia of WT cells by SEM (*Figure 4C*). We then analyzed the ultrastructure of the mouse trachea cilia by transmission electron microscope (TEM). In *Foxj1*$^{c.1129delT/c.1129delT}$ mice, classical motile type cilia with a clearly defined 9+2 microtubule doublets ultrastructure were entirely destroyed in tracheal cells, but only about 23% (14 of 54 cilia) of tracheal cilia from *Foxj1*$^{+/c.1129delT}$ mouse showed a disorganized arrangement of the microtubule doublets by counting 20 TEM images from two mice (*Figure 4D*). Collectively, those results show that *Foxj1*-c.1129delT knock-in mutation affects microtube orientation and ciliogenesis.

Transcriptomic analyses of Foxj1 mutant mouse heart tissues

To investigate the clues associated with abnormal heart phenotype in the proband, we performed RNA-Seq with P1 WT and *Foxj1*$^{c.1129delT/c.1129delT}$ mouse heart tissue. A total of 667 genes showed changes (differentially expressed genes, DEGs) in expression in the *Foxj1*$^{c.1129delT/c.1129delT}$ compared with their expression in the WT, including 432 up-regulated genes (64.8%) and 235 down-regulated genes (35.2%) (*Figure 5A* and available online https://cdn.amegroups.cn/static/public/tp-23-27-1.xls). The Gene Ontology (GO) functional analysis of the DEGs was divided into the biological process (BP), molecular function (MF) and cell component (CC). The top 15 results obtained from the GO enrichment analysis of the up-regulated and down-regulated DEGs are shown in *Figure 5B*, website: https://cdn.amegroups.cn/static/public/tp-23-27-2.xls and website: https://cdn.amegroups.cn/static/public/tp-23-27-3.xls. The up-regulated genes were mainly enriched in response to virus/immune process (Ontology: BP), the stress fiber/Z disc (Ontology: CC), and protein binding/cytokine activity (Ontology: MF) and the down-regulated genes were mainly enriched in potassium ion transport/transcription regulation, T-tubule/sarcolemma and (phospho-) lipid transporter activity/nucleotide (DNA) binding, respectively. The top 30 KEGG pathways for DEGs are shown in *Figure 5C* and website: https://cdn.amegroups.cn/static/public/tp-23-27-4.xls, which contain human diseases such as hypertrophic cardiomyopathy and dilated cardiomyopathy. In addition, pathway "adrenergic signaling in cardiomyocytes" was enriched among genes commonly down-regulated in *Foxj1* mutant heart tissue (*Figure 5D*). These preliminary results may provide clues for the associations between *Foxj1* and heart disease.

Discussion

In this study, we identified a novel heterozygous deletion mutation (c.1129delC/p.Leu377Trpfs*76) of *FOXJ1* in one Chinese family with situs inversus, and the proband is complicated with complex congenital heart disease (CHD). This mutant p.Leu377Trpfs*76 protein, expressed with an almost equal level of the WT and localized normally in the nucleus, shows a dominant-negative effect on the expression of *RFX3 in vitro*. Moreover, we generated the first *Foxj1* knock-in (c.1129delT, ortholog of the c.1129delC in human *FOXJ1*) mice that recapitulated the situs anomalies of our patients. Together, we report maternally inherited and a heterozygous dominant *de-novo* mutation in *FOXJ1* with type 43 primary ciliary dyskinesia (CILD43, OMIM#618699). Additionally, transcriptome data of *Foxj1* knock-in mouse hearts suggest that we should be aware of cardiac anomalies in individuals with *FOXJ1* variants.

Even though *Foxj1* null mice are well known for their abnormalities in left-right axis determination over two decades (11,13), the *FOXJ1* mutations concerning human disorders are just identified over the past several years (3). To date, only eight *FOXJ1* mutations have been reported, of which one is an amino acid substitution and seven are premature termination products on protein sequence, in 12 individuals (Table S2). Collectively, exon 3 of *FOXJ1* seems to be a mutational hotspot and the majority of pathogenic variants were nonsense or frameshift type. The C-terminal region of FOXJ1 contains a transactivation region and removing the fourth acidic domain causes a significant decrease in its transcriptional activity (10). Consistent with this study, we found that c.1129delC alteration, predicted to disrupt the A4 region of FOXJ1, reduced its transcriptional activity on *RFX3* via a dominant negative mechanism. Similar to our findings, action models like *FOXJ1*-c.1129delC mutation have been reported in other forkhead transcription factors. For example, *Foxo1* lacking the C-terminal transactivation domain could act in a dominant-negative manner (21) and dominant-negative mutant of *FOXE3* with an autosomal-dominant trait contributes to human ocular disease (22). However, the only functional study carried out so far indicates haploinsufficiency being the disease cause by 3'mRNA-seq of air-liquid interface-cultured respiratory epithelial cells from two controls and two *FOXJ* mutant individuals (3). Thus, it would be helpful to further test this dominant negative mutant *in vivo* by using *Foxj1* knock-out and *Foxj1*-c.1129delT knock-in mouse models, and more research is needed to understand the action mechanism of *FOXJ1* variants.

FOXJ1 is the master regulator of the transcriptional program that drives the assembly of motile cilia. Abnormal ciliary structure and function in *Foxj1* deficient model organisms are considered as the causative of *Foxj1*-related disorders (11,23). In our study, heterotaxy and the rough breathing sounds of both lungs presented in the patients implied an impairment of the node cilia cells and ciliated pulmonary epithelial cells. Similarly, our *Foxj1*-c.1129delT knock-in mice presented with randomization of left/right body asymmetry. As expected, the number and density of tracheal cilia from *Foxj1*-c.1129delT mutant mice were reduced and cilia were disorganized

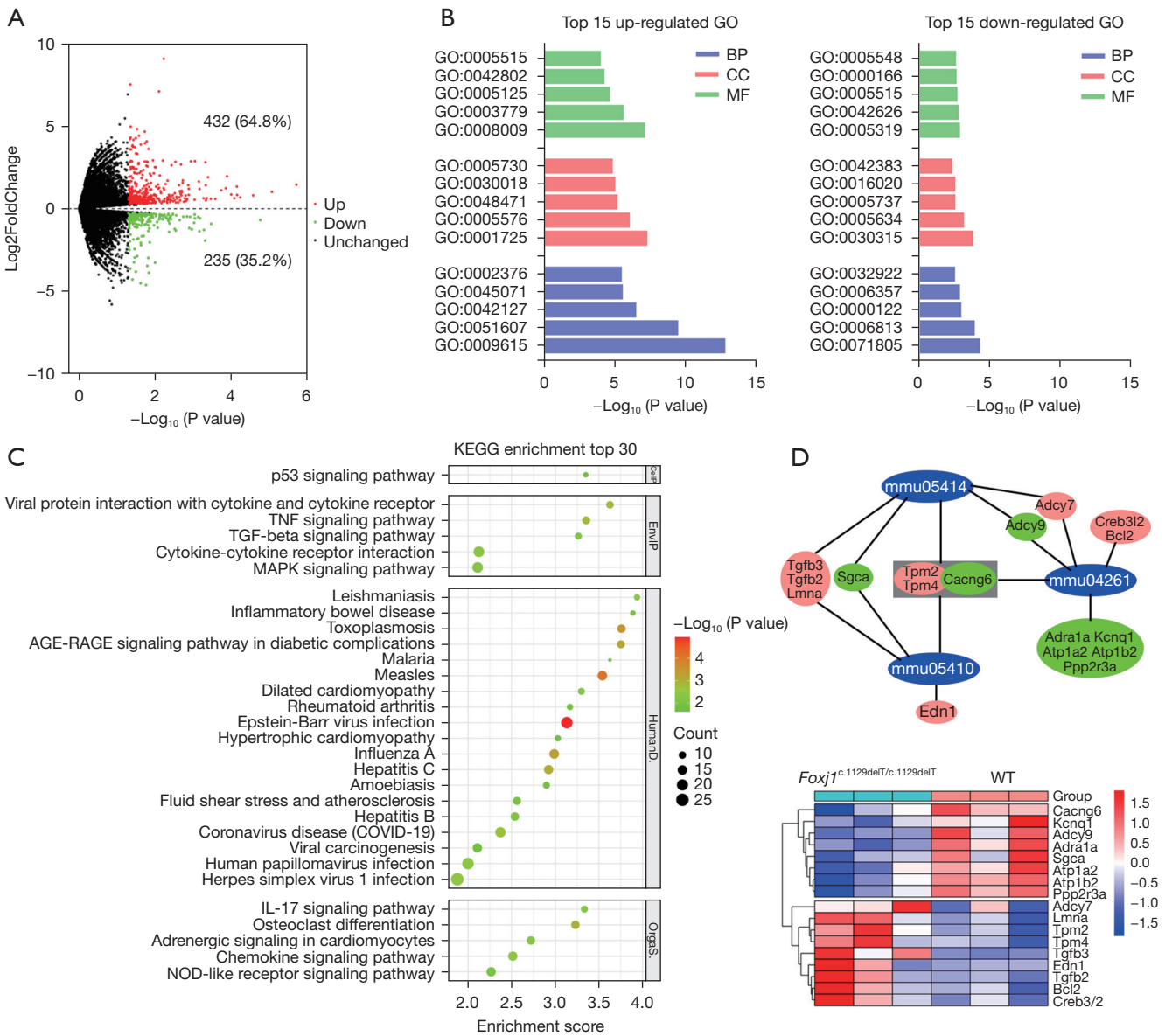

Figure 5 Transcriptome profiling of wild-type and *Foxj1*$^{c.1129delT/c.1129delT}$ mutant mouse heart tissues. (A) Volcano plot displaying the gene expression for *Foxj1*$^{c.1129delT/c.1129delT}$ *vs.* WT mouse heart tissues. The up/down-regulated genes based on P<0.05 and |log2FoldChange| >0.26. (B) Up/down-regulated DEGs with the top 15 enriched GO terms. (C) The KEGG pathway enrichment analysis of the DEGs. Top 30 KEGG pathways enrichment analysis of the DEGs ranked by P value, involving 1 CellP, 5 EnvIP, 19 HumanD and 5 OrgaS. (D) Network map of enriched pathways. Blue represents the pathways (mmu05414: dilated cardiomyopathy, mmu05410: hypertrophic cardiomyopathy, mmu04261: adrenergic signaling in cardiomyocytes). Genes in the red and green boxes are up-regulated and down-regulated, respectively. The cluster heat map shows the expression levels of genes involved in the three pathways in two groups. GO, Gene Ontology; BP, biological process; CC, cell component; MF, molecular function; KEGG, Kyoto Encyclopedia of Genes and Genomes; TNF, tumor necrosis factor; TGF, transforming growth factor; MAPK, mitogen-activated protein kinases; AGE-RAGE, advanced glycation end products-receptor for advanced glycation end products; NOD, nucleotide-binding and oligomerization domain; WT, wild-type; DEGs, differential expression genes; CellP, cellular process; EnvIP, environmental information processing; HumanD, human diseases; OrgaS, organismal systems.

along the surface of tracheal epithelial cells. The typical 9+2 cilia axoneme ultrastructure was entirely and partially destroyed in homozygous and heterozygous *Foxj1* knock-in mice, respectively. Ciliary cross sections of respiratory epithelial cells from *FOXJ1* affected individuals exhibited variable cilia structural defects, and some did not show any abnormalities of the 9+2 axonemal architecture. However, the number of cells with normal amounts of cilia in all sufferers was reduced. These affected individuals have an associated mucociliary clearance disorder, but only half have situs inversus (3). Thus, we noted that foxj1 dysfunction is not causing a uniform ciliary ultrastructure abnormality, but rather a decreased number and random changes in organization. Meanwhile, the proband's mother was unable to conceive naturally. These reduced fertility conditions have been earlier reported in three patients with *FOXJ1* mutation. One was unable to become pregnant, one had hydrosalpinx, and one male had severe oligoasthenoteratospermia (Table S2). In a mouse model, attempts on mating male or female *Foxj1*$^{-/-}$ mice with productive WT counterparts were unsuccessful (13). These data suggest that *FOXJ1* mutation might influence ciliogenesis in the female reproductive tract and sperm flagella movement thereby affecting human fertility. Regretfully, *Foxj1*-c.1129delT knock-in mice died soon after birth, and the offspring number at birth was not evaluated. In addition, as shown in Table S2, hydrocephalus seems to be a fully penetrant condition from previously reported *FOXJ1* mutant patients. Even though this phenotype is not informed in our patient, dilated ventricles were observed in almost all *Foxj1*-c.1129delT knock-in mice. This prominent phenotype could be explained by specific or preferential *FOXJ1* expression in the brain ependymal cells, and defects in the ependymal cilia affect the cerebrospinal fluid passage during brain formation that led to hydrocephalus (24). Meanwhile, further detailed inspection is required to investigate the other common PCD-related symptoms and ciliary ultrastructure from the proband's mother. Collectively, these data demonstrated that heterozygous *Foxj1*-c.1129delT mutation could results in mouse ciliary ultrastructural defects and this model presents primary ciliary dyskinesia related phenotypes and mimics the clinical symptoms of our patient.

In addition, another remarkable aspect, severe and complex CHD, is presented in the proband. Although assisted reproduction technologies have also been associated with higher risk of birth defects, such as congenital heart defects (25). Interestingly, CHD phenotypes were mentioned in other two cases with *FOXJ1* variants, one presented with a ventricular septal cardiac defect and another with a small atrial septal defect (TableS 2). Besides, we screened two rare and predicted damaging *FOXJ1* variants (c.266G>A/p.Gly89Asp, Exon2; c.637C>T/p.Arg213Trp, Exon3) in our cohort of patients with Tetralogy of Fallot (Table S3 and Figure S2). RNA-seq on cardiac cell line AC16 overexpressing wild-type or p.Arg213Trp mutant of *FOXJ1* were performed and found that enriched KEGG pathways of down-regulated DEGs included the calcium signaling pathway and adrenergic signaling in cardiomyocytes, which is important for early gene expression of myocardial cells, and cardiomyocyte maturation and apoptosis (26,27) (Table S4). Similarly, cardiomyopathy-associated genes are differentially expressed [e.g., Tpm2/3 (28); Tgfb2/3 (29)] and adrenergic signaling in cardiomyocytes pathway are enriched from the transcriptome results of *Foxj1* knock-in mouse heart tissues. While this does not exclude the possibility that these genetic changes result from structural cardiac anomalies rather than a direct Foxj1 effect. To date, the relationship between *FOXJ1* variants and CHD is barely known, our preliminary findings may provide new information on the association between CHD and *FOXJ1*. Although hydrocephalus is common in animals with primary ciliary dyskinesia (PCD), these models distinctly have an increased incidence of CHD (30,31). Hence, CILD43 patients should be aware of the cardiac abnormality and CHD individuals could test for *FOXJ1* variants.

In our report, both *Foxj1*$^{c.1129delT/c.1129delT}$ and *Foxj1*$^{+/c.1129delT}$ mice developed situs inversus and hydrocephalus, and showed a disruption of trachea cilia structure, whereas these abnormalities are only observed in previous reported *Foxj1*$^{-/-}$ mice and no aberration existed in single *Foxj1* allele deletion (*Foxj1*$^{+/-}$) mice. *Foxj1*$^{-/-}$ mice all died within postnatal days 40 (P40) and approximately half of the born had situs inversus and hydrocephalus (11,13). However, our *Foxj1*$^{c.1129delT/c.1129delT}$ mice seem to have a higher proportion reversal of internal organs, die earlier, and almost all mice developed hydrocephalus, though the numbers of mice examined was insufficient to reflect the proper incidence of situs inversus for *Foxj1*-c.1129delT mice early death. The proband died from severe CHD. Collectively, mice with c.1129delT mutation in *Foxj1* showed a severer phenotype than *Foxj1* allele deletion, which reflects a potential toxicity effect of the existence of aberrant Foxj1. In addition, hydrocephalus impacts the fundamental aspects of brain development, associated phenotypes such as intellectual disability and neurodevelopmental delay are not infrequent findings among

patients (4), but the developmental delay simply told in three patients with congenital hydrocephalus who carry a *FOXJ1* mutation (Table S2). And growth failure was observed in *Foxj1*$^{-/-}$ (13) and our *Foxj1*$^{+/c.1129delT}$ mice. In summary, *Foxj1*-c.1129delT knock-in mice generally showed the same traits as *Foxj1*$^{-/-}$ mice, but produced more severe effects, implying an adverse consequence of *Foxj1*-c.1129delT mutants.

Conclusions

Our findings expand the clinical and mutational spectrum of type 43 primary ciliary dyskinesia caused by mutations in *FOXJ1*. Meanwhile, much work remains to be done in unraveling the pathogenesis of *FOXJ1* mutations. Identifying more patients with *FOXJ1* variant will be toward a comprehensive understanding of the genotype-phenotype relationships and provide valuable diagnosis data. More distinct forms of *Foxj1* knock-in mice can help to elucidate the mechanism underlying various clinical traits.

Acknowledgments

We would like to thank the patients and their family members for participating in this study.

Funding: The work was supported by National Key R&D Program of China (No. 2021YFC2701104), National Natural Science Foundation of China (No. 82001565), Science and Technology Commission of Shanghai Municipality (No. 21Y31900301), the Collaborative Innovation Program of Shanghai Municipal Health Commission (2020CXJQ01), and Shanghai Natural Science Foundation Project (No. 20ZR1434800).

Footnote

Reporting Checklist: The authors have completed the ARRIVE reporting checklist. Available at https://tp.amegroups.com/article/view/10.21037/tp-23-27/rc

Data Sharing Statement: Available at https://tp.amegroups.com/article/view/10.21037/tp-23-27/dss

Conflicts of Interest: All authors have completed the ICMJE uniform disclosure form (available at https://tp.amegroups.com/article/view/10.21037/tp-23-27/coif). The authors have no conflicts of interest to declare.

Ethical Statement: The authors are accountable for all aspects of the work in ensuring that questions related to the accuracy or integrity of any part of the work are appropriately investigated and resolved. The study was conducted in accordance with the Declaration of Helsinki (as revised in 2013). The study was approved by the Ethics Committee of the Shanghai Children's Medical Center (SCMC) (No. SCMC-201015) and written informed consent was obtained from the parents of the child. Experiments were performed under a project license (No. SCMC-LAWEC-2023-005) granted by institutional Animal Care and Use Committee of SCMC, in compliance with SCMC institutional guidelines for the care and use of animals.

References

1. Wallmeier J, Nielsen KG, Kuehni CE, et al. Motile ciliopathies. Nat Rev Dis Primers 2020;6:77.
2. Lucas JS, Davis SD, Omran H, et al. Primary ciliary dyskinesia in the genomics age. Lancet Respir Med 2020;8:202-16.
3. Wallmeier J, Frank D, Shoemark A, et al. De Novo Mutations in FOXJ1 Result in a Motile Ciliopathy with Hydrocephalus and Randomization of Left/Right Body Asymmetry. Am J Hum Genet 2019;105:1030-9.
4. Jin SC, Dong W, Kundishora AJ, et al. Exome sequencing implicates genetic disruption of prenatal neuro-gliogenesis in sporadic congenital hydrocephalus. Nat Med 2020;26:1754-65.
5. Shapiro AJ, Kaspy K, Daniels MLA, et al. Autosomal dominant variants in FOXJ1 causing primary ciliary dyskinesia in two patients with obstructive hydrocephalus. Mol Genet Genomic Med 2021;9:e1726.
6. Kundishora AJ, Singh AK, Allington G, et al. Genomics of human congenital hydrocephalus. Childs Nerv Syst 2021;37:3325-40.
7. Yu X, Ng CP, Habacher H, et al. Foxj1 transcription factors are master regulators of the motile ciliogenic program. Nat Genet 2008;40:1445-53.
8. Blatt EN, Yan XH, Wuerffel MK, et al. Forkhead

transcription factor HFH-4 expression is temporally related to ciliogenesis. Am J Respir Cell Mol Biol 1999;21:168-76.
9. Hackett BP, Brody SL, Liang M, et al. Primary structure of hepatocyte nuclear factor/forkhead homologue 4 and characterization of gene expression in the developing respiratory and reproductive epithelium. Proc Natl Acad Sci U S A 1995;92:4249-53.
10. Lim L, Zhou H, Costa RH. The winged helix transcription factor HFH-4 is expressed during choroid plexus epithelial development in the mouse embryo. Proc Natl Acad Sci U S A 1997;94:3094-9.
11. Brody SL, Yan XH, Wuerffel MK, et al. Ciliogenesis and left-right axis defects in forkhead factor HFH-4-null mice. Am J Respir Cell Mol Biol 2000;23:45-51.
12. Stauber M, Weidemann M, Dittrich-Breiholz O, et al. Identification of FOXJ1 effectors during ciliogenesis in the foetal respiratory epithelium and embryonic left-right organiser of the mouse. Dev Biol 2017;423:170-88.
13. Chen J, Knowles HJ, Hebert JL, et al. Mutation of the mouse hepatocyte nuclear factor/forkhead homologue 4 gene results in an absence of cilia and random left-right asymmetry. J Clin Invest 1998;102:1077-82.
14. Hagenlocher C, Walentek P, M Ller C, et al. Ciliogenesis and cerebrospinal fluid flow in the developing Xenopus brain are regulated by foxj1. Cilia 2013;2:12.
15. Beckers A, Adis C, Schuster-Gossler K, et al. The FOXJ1 target Cfap206 is required for sperm motility, mucociliary clearance of the airways and brain development. Development 2020;147:dev188052.
16. Didon L, Zwick RK, Chao IW, et al. RFX3 modulation of FOXJ1 regulation of cilia genes in the human airway epithelium. Respir Res 2013;14:70.
17. Bonnafe E, Touka M, AitLounis A, et al. The transcription factor RFX3 directs nodal cilium development and left-right asymmetry specification. Mol Cell Biol 2004;24:4417-27.
18. Liang F, Wang B, Geng J, et al. SORBS2 is a genetic factor contributing to cardiac malformation of 4q deletion syndrome patients. Elife 2021;10:e67481.
19. Richards S, Aziz N, Bale S, et al. Standards and guidelines for the interpretation of sequence variants: a joint consensus recommendation of the American College of Medical Genetics and Genomics and the Association for Molecular Pathology. Genet Med 2015;17:405-24.
20. Zhang X, Gao Y, Zhang X, et al. FGD5-AS1 Is a Hub lncRNA ceRNA in Hearts With Tetralogy of Fallot Which Regulates Congenital Heart Disease Genes Transcriptionally and Epigenetically. Front Cell Dev Biol 2021;9:630634.
21. Nakae J, Kitamura T, Silver DL, et al. The forkhead transcription factor Foxo1 (Fkhr) confers insulin sensitivity onto glucose-6-phosphatase expression. J Clin Invest 2001;108:1359-67.
22. Reis LM, Sorokina EA, Dudakova L, et al. Comprehensive phenotypic and functional analysis of dominant and recessive FOXE3 alleles in ocular developmental disorders. Hum Mol Genet 2021;30:1591-606.
23. Zhang M, Bolfing MF, Knowles HJ, et al. Foxj1 regulates asymmetric gene expression during left-right axis patterning in mice. Biochem Biophys Res Commun 2004;324:1413-20.
24. Olstad EW, Ringers C, Hansen JN, et al. Ciliary Beating Compartmentalizes Cerebrospinal Fluid Flow in the Brain and Regulates Ventricular Development. Curr Biol 2019;29:229-241.e6.
25. Wang C, Lv H, Ling X, et al. Association of assisted reproductive technology, germline de novo mutations and congenital heart defects in a prospective birth cohort study. Cell Res 2021;31:919-28.
26. Giacomelli E, Meraviglia V, Campostrini G, et al. Human-iPSC-Derived Cardiac Stromal Cells Enhance Maturation in 3D Cardiac Microtissues and Reveal Non-cardiomyocyte Contributions to Heart Disease. Cell Stem Cell 2020;26:862-879.e11.
27. Papa A, Kushner J, Marx SO. Adrenergic Regulation of Calcium Channels in the Heart. Annu Rev Physiol 2022;84:285-306.
28. Matyushenko AM, Levitsky DI. Molecular Mechanisms of Pathologies of Skeletal and Cardiac Muscles Caused by Point Mutations in the Tropomyosin Genes. Biochemistry (Mosc) 2020;85:S20-33.
29. Boileau C, Guo DC, Hanna N, et al. TGFB2 mutations cause familial thoracic aortic aneurysms and dissections associated with mild systemic features of Marfan syndrome. Nat Genet 2012;44:916-21.
30. Brueckner M. Heterotaxia, congenital heart disease, and primary ciliary dyskinesia. Circulation 2007;115:2793-5.
31. Sakamoto K, Nakajima M, Kawamura K, et al. Ependymal ciliary motion and their role in congenital hydrocephalus. Childs Nerv Syst 2021;37:3355-64.

Cite this article as: Li L, Shi G, Zhang X, Wang T, Wang B, Gao Y, You G, Fu Q, Xiang Y, Zhang X. Novel dominant-negative FOXJ1 mutation in a family with heterotaxy plus mouse model. Transl Pediatr 2023;12(8):1476-1489. doi: 10.21037/tp-23-27

Table S1 The primers used for validation of *FOXJ1* variants

Primers	Sanger sequencing (5'-3')
Gly89Asp	Forward: CTCCATTCTCAACGCCAAG
	Reverse: ATCTTGGTGGCCTTGCTG
Arg213Trp	Forward: CAAGTGCTTCATCAAAGTGC
	Reverse: AAGTTGCCTTTGAGGGGTTC
p.Leu377Trpfs*76	Forward: GAACCCCTCAAAGGCAACTT
	Reverse: CTAGGTGGTGGGGTGTCTGT

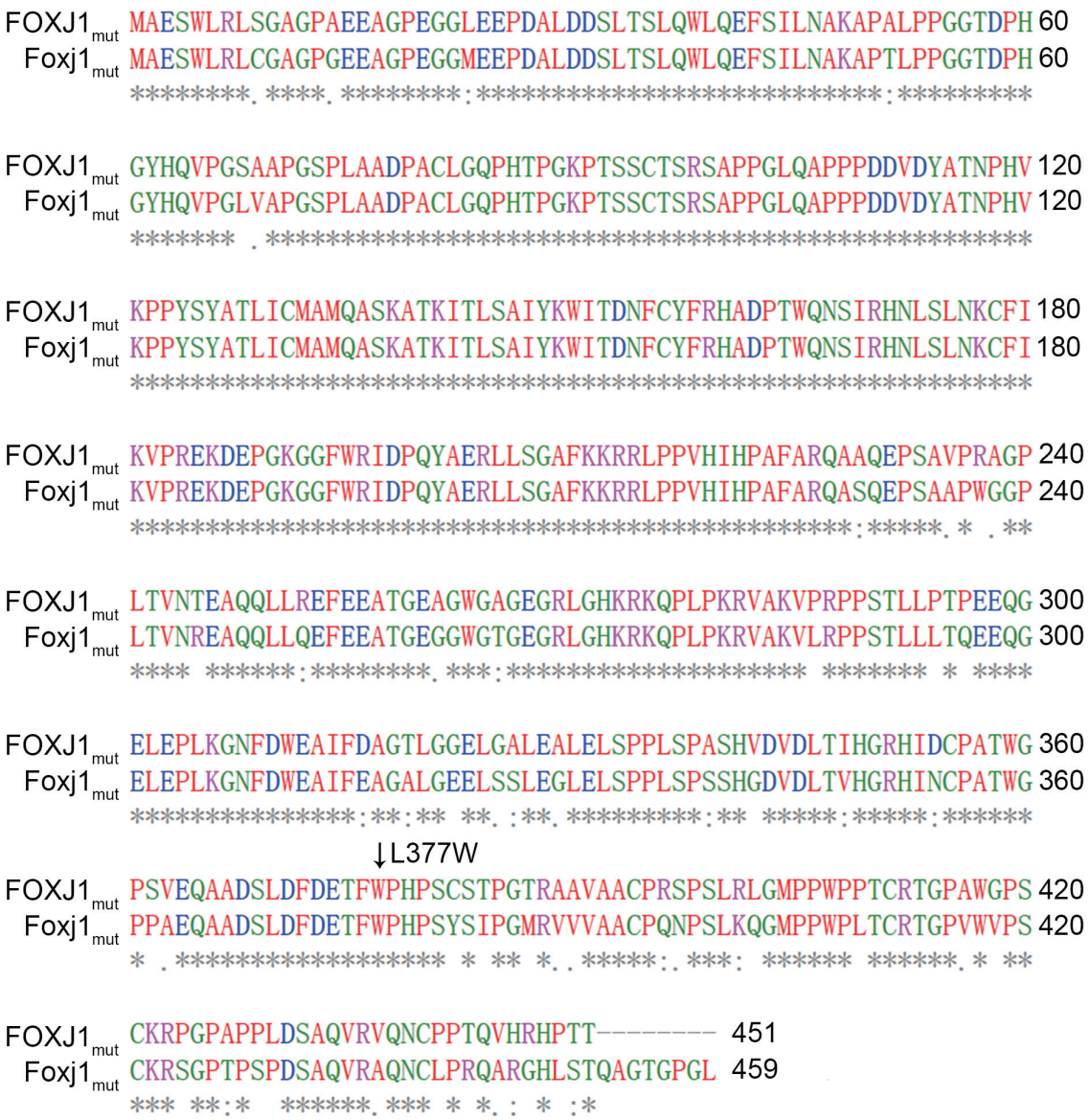

Figure S1 Amino acid sequence comparison of mutant human ($FOXJ1_{mut}$) and mouse ($Foxj1_{mut}$). Sequences were aligned using Clustal Omega, and the numbers indicate the positions of amino acid residues on the complete sequence alignment.

https://dx.doi.org/10.21037/tp-23-27

Table S2 Summary of previously published and this paper reported pathogenic variants in *FOXJ1*

Patient	Gender	Ethnicity	Nucleotide change	Location	Protein Change	Clinical features						Reference
						MCCD	hydrocephalus	CHD	Situs inversus	Fertility	Other phenotype	
OP-1743 II1	Male	Germany	c.901G>T	Exon3	p.Glu301*	+	+	–	–			(3)
OP-2950 II1	Female	Germany	c.868_871dup	Exon3	p.Thr291Lysfs*12	+	+	–	+	Infertility	Macrocephaly	
RBH II1	Female	Germany	c.967delG	Exon3	p.Glu323Serfs*10	+	+	–	–	Hydrosalpinx		
OP-1933 II1	Male	Germany	c.826C>T	Exon3	p.Gln276*	+	+	VSD	–			
US-1 II1	Male	USA	c.826C>T	Exon3	p.Gln276*	+	+	–	+			
US-2 II1	Male	USA	c.939delC	Exon3	p.Ile314Serfs*19	+	+	–	+	Subfertility		
KCHYD109-2[a]	Female	European	c.287C>G	Exon2	p.Thr96Arg	–	–	–	–	–		(4)
KCHYD109-1[b]	Male	European	c.287C>G	Exon2	p.Thr96Arg	–	+	–	–		Developmental delay	
KCHYD376-1	Male	European	c.826C>T	Exon3	p.Gln276*	–	+	–	–		Developmental delay	
KCHYD238-1	Female	European	c.967delG	Exon3	p.Glu323Serfs*10	–	+	–	–		Developmental delay	
UNC-1459	Female	Jewish	c.945delC	Exon3	p.Phe315Leufs*18	+	+	ASD	+			(5)
UNC-0852	Male	Irish/USA	c.929_932delACTG	Exon3	p.Asp310Glyfs*22	+	+	–	–	–		
II:2	Female	Chinese	c.1129delC	Exon3	p.Leu377Trp*fs76		–	–		Infertility		This paper
III:1	Male	Chinese	c.1129delC	Exon3	p.Leu377Trp*fs76	+	–	+		–		

MCCD, mucociliary clearance disorder; CHD, congenital heart disease; VSD, ventricular septal defect; ASD: atrial septal defect; a, b, mother-child relationship.

Table S3 In silico pathogenicity prediction of FOXJ1 variants

chr	hg19_pos	ref	alt	aaref	aaalt	rs_dbSNP	aapos	genename	Ensembl_geneid	Ensembl_transcriptid	Ensembl_proteinid	Uniprot_acc	SIFT_score	SIFT_pred	Polyphen2_HDIV_score	Polyphen2_HDIV_pred	Polyphen2_HVAR_score	Polyphen2_HVAR_pred	MutationTaster_score	MutationTaster_pred	CADD_phred	h1000Gp3_AF	UK10K_AF	ESP6500_AF	ExAC_AF	gnomAD_exomes_AF	gnomAD_genomes_AF
17	74136211	C	T	G	D	rs780094426	89	*FOXJ1*	ENSG00000129654	ENST00000322957	ENSP00000323880	Q92949	0.025	D	0.999	D	0.94	D	1	D	26.4	.	.	.	2.56E-05	.	.
17	74134063	G	A	R	W	rs764249412	213	*FOXJ1*	ENSG00000129654	ENST00000322957	ENSP00000323880	Q92949	0	D	1	D	1	D	1	D	27	.	.	.	1.65E-05	4.27E-06	6.57E-06

https://dx.doi.org/10.21037/tp-23-27

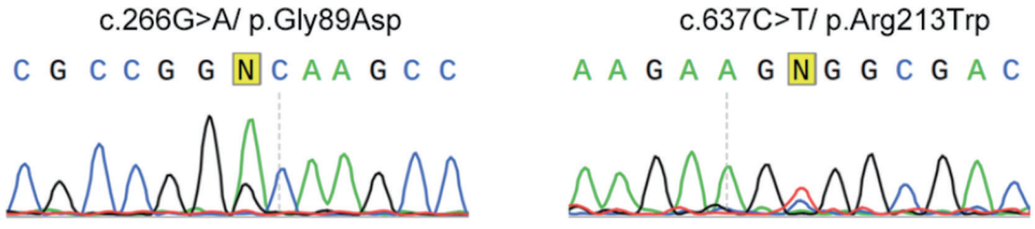

Figure S2 DNA sequence chromatographs confirming the heterozygous alteration in *FOXJ1*.

Table S4 The Kyoto Encyclopedia of Genes and Genomes (KEGG) pathway results of down-regulated genes in *FOXJ1*-c.637C>T overexpressed AC16 cells

Category	Term	Count	%	PValue	Genes	List Total	Pop Hits	Pop Total	Fold Enrichment	Bonferroni	Benjamini	FDR
KEGG_PATHWAY	hsa04970: salivary secretion	4	5.79710145	6.97E-04	*GUCY1A2*, *CHRM3*, *CALML6*, *ATP2B2*	17	92	8164	20.8797954	0.06673378	0.069040701	0.069040701
KEGG_PATHWAY	hsa04020: calcium signaling pathway	4	5.79710145	0.01058194	*CHRM3*, *CALML6*, *CACNA1A*, *ATP2B2*	17	240	8164	8.003921569	0.65117839	0.523806164	0.523806164
KEGG_PATHWAY	hsa04261: adrenergic signaling in cardiomyocytes	3	4.34782609	0.03399868	*CALML6*, *ATP2B2*, *CACNA2D4*	17	150	8164	9.604705882	0.96743177	0.819035304	0.819035304
KEGG_PATHWAY	hsa04921: oxytocin signaling pathway	3	4.34782609	0.0356801	*GUCY1A2*, *CALML6*, *CACNA2D4*	17	154	8164	9.355233002	0.97259109	0.819035304	0.819035304
KEGG_PATHWAY	hsa04022: cGMP-PKG signaling pathway	3	4.34782609	0.04136542	*GUCY1A2*, *CALML6*, *ATP2B2*	17	167	8164	8.626981331	0.98473643	0.819035304	0.819035304

FDR, false discovery rate.

https://dx.doi.org/10.21037/tp-23-27